L_3 Phase in a Binary Block Copolymer/Water System

E. Hecht,[†] K. Mortensen,[‡] and H. Hoffmann*,[†]

Physical Chemistry I, University of Bayreuth, 95440 Bayreuth, Germany, and Department of Solid State Physics, Risø National Laboratory, DK-4000 Roskilde, Denmark

Received April 4, 1995; Revised Manuscript Received May 23, 1995[⊗]

ABSTRACT: Block copolymers of the Poloxamer type $EO_xPO_yEO_x$ (with EO = ethylene oxide and PO = propylene oxide) can form lyotropic liquid crystalline phases in water, as is known for small hydrocarbon surfactants. The phase behavior of PE6200 (EO_6−PO_{36}−EO_6) is investigated in more detail for concentrations up to 50 wt % and temperatures from 0 to 100 °C. The technical product contains about 10 wt % hydrophobic contaminations, which induce clouding at ambient temperatures. These "impurities" can be removed by filtration, but they do not affect the subsequent phase behavior. A lamellar phase (L_α) and a spongelike phase (L_3) are found and characterized by DSC, SANS, electric birefringence, dynamic light scattering, and specific conductivity. The temperatures for the phase transitions decrease linearly with increasing NaCl concentration. In the L_3 phase the orientational relaxation time from electric birefringence decreases with the third power of the volume fraction and the reduced diffusion coefficient derived from dynamic light scattering increases linearly with Poloxamer concentration. The conductivity of added electrolyte clearly shows the bicontinuous structure of the Poloxamer L_3 phase. Comparison of the systems PE6200/water and $C_{12}EO_5$/water shows analogies for the phase behavior and the properties in the different phases.

1. Introduction

Block copolymers of the Poloxamer type $EO_xPO_yEO_x$ (with EO = ethylene oxide and PO = propylene oxide), also called Pluronics or Synperonics, have found wide technical application.[1] Above the critical micelle concentration (cmc, at constant temperature), or the critical micelle temperature (cmt, at constant concentration), they form micelles with a hydrophobic core of PO blocks and a highly swollen shell of EO blocks.[2−12] Like normal hydrocarbon surfactants Poloxamers can form lyotropic liquid crystals like the lamellar, hexagonal, and cubic phase.[3−5,7,8,12] The micellar properties can directly be controlled by the EO/PO ratio, the molecular weight, and the temperature.[6,11,12] At constant EO block size the increase of the PO block length decreases both the cmc and cmt. Keeping the PO block size constant and increasing the EO block length increases the cmc and cmt. With a constant EO/PO ratio an increase of the overall molecular weight again decreases the cmc and cmt.[11,12]

The aggregation behavior of Poloxamers is much more temperature dependent than that of nonionic surfactants C_nEO_x.[12,13] As has been shown by Alexandridis et al.[11] and Wanka et al.,[12] the surface area A of Poloxamers at the air/water interface decreases with increasing temperature, which is in contrast to hydrocarbon surfactants. This decrease of A has been explained by a dehydration of the EO blocks, which induces a more compact packing of the copolymer molecules at the interface, or an increasing hydrophobicity of the PO blocks.[11] Thus, the curvature of Poloxamer aggregates can be changed by varying the temperature. Wanka et al.[12] showed that for 35 wt % P104 ($EO_{18}PO_{58}EO_{18}$) the phase sequence micellar → cubic → hexagonal and for 60 wt % P65 ($EO_{20}PO_{30}EO_{20}$) the sequence micellar → hexagonal → lamellar can be induced only by increasing the temperature.

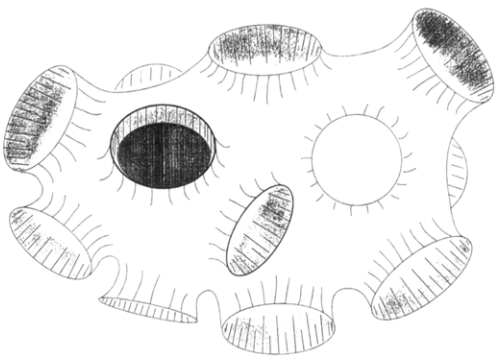

Figure 1. Schematic drawing of the bicontinuous L_3 (sponge) phase.

For ionic surfactants the spontaneous mean curvature of the aggregates can be influenced by addition of electrolyte or cosurfactant.[14−18] At low cosolute concentrations the curvature of the polar/apolar interface is toward the hydrophobic tails; hence, spherical micelles (L_1) are formed. With increasing cosolute concentration the curvature decreases and rodlike micelles are formed, until the spontaneous mean curvature is zero, resulting in the formation of flat lamellae (L_α). Further addition of cosolute leads to a curvature toward the solvent, which is an important condition for the formation of the L_3 phase.[15] This L_3 phase (also called "sponge phase") has a three-dimensional structure of continuous bilayers (Figure 1). With increasing curvature toward the solvent, the formation of the L_2 phase is induced, which contains inverted micelles with a hydrophilic core of hydrated headgroups and a hydrophobic shell of the hydrocarbon tails.

A similar behavior has been observed for binary mixtures of water and nonionic surfactants of the type C_nEO_x.[13] As these solutions show temperature-dependent aggregation behavior, the spontaneous curvature of the polar/apolar interface also can be controlled by the temperature. Hence, temperature is the third parameter like salt or cosurfactant concentration in the case of ionic surfactants + water. In close analogy to the case of ionic surfactant/cosurfactant (or salt)/water the phase sequence $L_1 \rightarrow L_\alpha \rightarrow L_3 \rightarrow L_2$ in the case of

* To whom correspondence should be addressed.
[†] University of Bayreuth.
[‡] Risø National Laboratory.
[⊗] Abstract published in *Advance ACS Abstracts,* July 1, 1995.

0024-9297/95/2228-5465$09.00/0

nonionic surfactants can be achieved by increasing the temperature. Only an intermediate EO block size permits the formation of the bilayer structure, e.g., $C_{12}EO_3$, $C_{12}EO_4$, $C_{12}EO_5$, $C_{12}EO_3$, $C_{16}EO_3$, and $C_{16}EO_4$.[13]

As expected from similar curvature of the bilayers, the L_3 phase always is adjacent to the lamellar phase L_α. As Strey et al.[19,20] found for a purified sample of $C_{12}EO_5$ (purity = 99.2%), the L_3 phase can be diluted down to a concentration of 0.5 wt % $C_{12}EO_5$ without leaving the phase. Also the L_α phase remains stable down to 1 wt % surfactant. The phase boundaries of the one-phase regions, however, strongly depend on the amount of impurities. The L_α phase of an unpurified sample of $C_{12}EO_5$ (purity ca. 98%) only can be diluted down to ca. 25 wt % surfactant, whereas the L_3 phase only can be diluted down to 4 wt %.[13]

For nonionic surfactants of the Poloxamer type a similar behavior should be expected. Indeed the phase diagrams of $C_{12}EO_x$ and Poloxamers show similar phase sequences as described above.[12,13] Poloxamers with a large headgroup are forced to aggregate in spherical micelles, as is the case for low temperatures. Decreasing the headgroup area by increasing the temperature now decreases the curvature of the aggregates, allowing the formation of rodlike micelles. At sufficiently high concentration these rods are organized in a hexagonal phase. Further increase of the temperature again decreases the surface area of the Poloxamer, so that flat lamellae can be formed. The lamellar phase, however, is restricted to Poloxamers with a low content of EO (10–50 wt %). For higher EO content the high surface area of the EO block cannot be compensated by an increase of temperature. Thus these Poloxamers only form cubic gels consisting of copolymer micelles arranged in a cubic lattice.

In the present investigation we want to give evidence that Poloxamers with an appropriate EO/PO ratio also can form L_3 phases. To our knowledge, this is the first time that L_3 phases are found for Poloxamers with a relatively broad distribution of composition and molecular weight. In most of the cases L_3 phases are formed by well-defined surfactant (/cosurfactant) systems with a uniform hydrocarbon chain length, which allows a constant bilayer thickness.[17] In the case of Poloxamers, however, the hydrophobic PO blocks show a distribution of block lengths; i.e., the formation of bilayers with constant thickness should be less probable. As mentioned above, an intermediate or even low content of hydrophilic EO is essential to allow the formation of the L_3 phase. Also the molecular weight of the Poloxamer has to be of intermediate size, because an increase of MW favors the formation of the cubic gel phase.[12] For these reasons Pluriol PE6200 has been selected to proof the existence of the L_3 phase in binary Poloxamer/water solutions.

2. Experimental Section

2.1. Materials. Pluriol PE6200 (MW = 2600, 20 wt % EO according to the manufacturer, corresponding to $EO_6PO_{36}EO_6$, which is similar to Pluronic L62 and Poloxamer 182 = $EO_5PO_{30}EO_5$) was obtained from BASF. All solutions were prepared by weight in twice-distilled water with pH ≅ 5 or in D_2O (Roth, Germany) for SANS measurements. The volume fraction of PE6200 has been calculated with the densities for H_2O, D_2O, and PE6200 to be 0.998, 1.007, and 1.007 g/mL, respectively. NaCl (p.a.) was supplied by Merck, Germany.

2.2. Phase Diagram. All solutions were prepared by weight and sealed in glass tubes, which were immersed in a thermostated water bath. At 0 °C all solutions were liquid and showed no turbidity. To scan the temperature behavior, the temperature was increased by steps of 2 °C, with each temperature kept constant at least 6 h. In the liquid crystalline region the thermostated time was prolonged to more than 1 day and the temperature intervals were reduced to 1 °C. Especially, the L_3 phase with its small one-phase region is very sensitive to temperature fluctuations and needed some time to reestablish again. Between crossed polarizers the solutions were examined macroscopically and the tubes were rotated or turned upside down to check for flow birefringence. The reproducibility of the phase boundaries was checked by several temperature scans and found to be ±1 wt % and ±1.5 °C.

2.3. Differential Scanning Calorimetry (DSC). Measurements were made with a Setaram Micro DSC in the temperature range between 0 and 100 °C. Dilute aqueous solutions of Poloxamers show an endothermic transition peak on heating and an exothermic peak on cooling. For the slow scanning rate of 0.2 K/min the two peaks are at the same temperature and show no kinetic retardation. T_{min} is the temperature in the peak minimum of the heating cycle. The onset temperature (T_{onset}) is defined as the temperature at the intersection of the tangent at the first inflection point of the peak with the baseline.

2.4. Small-Angle Light Scattering. The small-angle light scattering at $\theta = 6-7°$ was determined by a Chromatix KMX-6 photometer and a He/Ne laser. The solutions were filtered through a Schleicher & Schuell filter with 0.2 μm pore size before measurement. To remove the hydrophobic contaminations, the solution at $T >$ CP was filtered through a Schleicher & Schuell filter with 50 nm nominal pore size.

2.5. ^{1}H NMR. To analyze the composition of the block copolymers, a Bruker ARX 250 NMR was used at 250 MHz and T = 298 K. The solutions were prepared in $CDCl_3$ with concentrations of about 10%, and the resonance of $CHCl_3$ at δ = 7.24 ppm has been taken as internal reference.

2.6. Gel Permeation Chromatography (GPC). The distribution of particle sizes was analyzed by a gel permeation approach for oligomers (Waters) at T = 30 °C. Three Ultrastyragel columns with nominal pore sizes of 100, 500, and 1000 Å were switched in series with a mean particle size of 7 μm. The column was calibrated with a polystyrene standard so that no absolute values for the molecular weight could be observed. The refractive index was taken to detect the block copolymer. All solutions (10 g/L) were prepared in $CHCl_3$, which suppresses micellization, as evidenced by dynamic light scattering experiments.

2.7. Small-Angle Neutron Scattering (SANS). Small-angle neutron scattering experiments were performed using the Risø–SANS facility, which is a flexible instrument covering scattering vectors from 0.002 to 0.5 Å^{-1}, with variable neutron wavelength resolution. The scattering results presented below were obtained using neutrons with 3, 6, and 10 Å wavelength, with sample-to-detector distances of 1 and 3 m giving scattering vectors in the range 0.005–0.2 Å^{-1}, where the scattering vector q is given by the scattering angle θ and the neutron wavelength λ:

$$|\bar{q}| = q = \frac{4\pi}{\lambda}\sin\left(\frac{\theta}{2}\right) \quad (1)$$

The used neutron wavelength resolution was $\Delta\lambda/\lambda = 0.18$, the neutron beam collimation was determined by the pinhole sizes of 16 and 8 mm diameter at source and sample positions, respectively, and the collimation length was equal to the sample-to-detector distance. The smearing induced by the wavelength spread, the collimation, and the detector resolution was included in the data analysis discussed below, using Gaussian approximations for the different terms.[21] The samples were mounted in sealed quartz containers (Suprasil from Hellma, FRG), with 2 mm flight path.

The scattering data were corrected for the background arising from the quartz cell with D_2O and from other sources, as measured with the neutron beam blocked by plastic containing boron at the sample position. The incoherent scattering from H_2O was used to determine deviations from a uniform detector response and to convert the data into absolute units.

The scattering patterns were all azimuthally isotropic. The data have therefore by azimuthal averaging been reduced to the one-dimensional $I(q)$ scattering function which is only

dependent on the absolute value of $\bar{q}$. The temperature was controlled to within 1 °C using a Peltier device.

2.8. Electric Birefringence. In the L_3 one-phase region PE6200 solutions are isotropic and become birefringent either under shear or by applying an electric field. For the electric birefringence measurements a high-power pulse generator Cober Model 606 was used in the one-shot mode, providing rectangular dc pulses with a pulse width of 0.1−10 ms and an electric field up to 10^5 V/m. As a light source a He/Ne laser was used and all data were collected by a Datalab transient recorder DL920. The solutions were filled in a quartz cuvette and thermostated for at least 1 h. To be sure that no traces of L_α phase were present, the static birefringence had to approach zero.

2.9. Dynamic Light Scattering. To determine the cooperative diffusion coefficient in the L_3 phase, a 30-mW He/Ne laser with a Brookhaven BI-DS 10369 photomultiplier and a BI-8000 AT advanced digital correlator was used. All solutions were filtered at 4 °C (below the 2Φ region) through a Schleicher & Schuell filter with 0.2 μm pore size and were thermostated at the corresponding temperature for at least 1 h. To ensure the absence of a second phase, another sample of the same concentration was kept at the same temperature and checked for static birefringence between crossed polarizers. From the autocorrelation curve, a mean relaxation time τ_D can be obtained. Knowing the scattering vector q, we can calculate the effective diffusion coefficient D_{eff} (eq 2), which contains the structure factor $S(q)$ (eq 3) and corresponds to a translational cooperative diffusion rather than to a translational self-diffusion.

$$\tau_D = (q^2 D_{eff})^{-1} \quad (2)$$

$$D_{eff} = D_0/S(q) \quad (3)$$

2.10. Specific Conductivity. The specific conductivity was measured with a WTW Microprocessor Conductivity Meter LF2000 and a LTA electrode with a cell constant of 1.054 cm^{-1}. The solutions were filled in a thermostated glass cell and stirred during heating; to avoid evaporation, the whole cell assembly was closed. Especially in the liquid crystalline region the stirrer was switched off several minutes before the measurements were taken.

3. Results and Discussion

3.1. Phase Behavior. In the following we examine the detailed phase behavior of PE6200 in the concentration region up to 50 wt %. Figure 2 shows a cut of the investigated temperature range from 0 up to 100 °C. As at temperatures above 60 °C no further changes occur, this region is omitted to present the phase diagram more clearly. At low temperatures all solutions are isotropic and clear. With increasing temperature clouding occurs (2Φ), with CP decreasing with increasing concentration. For concentrations above 38 wt %, however, no clouding occurs, even if the solutions were thermostated for several days. Above 10 wt % PE6200 the solutions again become clear, when the temperature is raised. At temperatures higher than 40 °C an additional phase is formed at the bottom of the tubes. It shows strong birefringence and has a relatively high viscosity, but it is still liquid. On the basis of its texture under the polarizing microscope, it is a lamellar phase L_α. With increasing concentration the viscosity in the one-phase L_α region increases. The solutions with low concentrations show a bluish color, and the same holds for the isotropic one-phase region below. Above the L_α phase a two-phase region appears with a milky opalescent phase on top of the samples. In the one-phase region this phase is isotropic and shows flow birefringence over the entire concentration range. The viscosity is slightly above that of water and markedly below that of the L_α phase. It will be proven below that this phase corresponds to the L_3 or spongelike phase. Above the

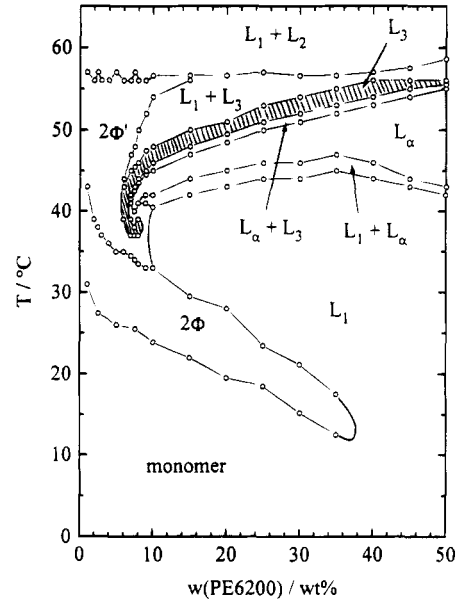

Figure 2. Phase diagram of the system PE6200 ($EO_6PO_{36}EO_6$)/water. L_1 and L_2 denote isotropic liquid solutions, L_3 is the isotropic spongelike phase, and L_α is the lamellar liquid crystalline phase; for 2Φ and 2Φ′, see text.

L_3 one-phase region an additional isotropic phase with low viscosity is formed on top of the samples, which is attributed to the micellar L_1 phase. At temperatures above 57 °C all samples show a two-phase region with a polymer-rich phase at the bottom and a water-rich phase at the top of the samples. Both phases are isotropic and do not show any flow birefringence. Also the milky opalescence of the L_3 phase has disappeared, which can be used to detect the phase transition. Analogous to binary phase diagrams for C_nEO_x/water,[13,19] these phases are called L_1 for the water-rich phase and L_2 for the polymer-rich phase. With further increase of temperature up to 100 °C, no changes occur over the whole investigated concentration range.

Below 10 wt % PE6200 the phase behavior differs somewhat from the more concentrated region. With increasing temperature at first the cloud point is exceeded and two isotropic liquid phases are formed (2Φ). For $C_{12}EO_5$/water, which shows some similarities to the PE6200/water system, Strey et al.[19] called this two-phase region $L'_1 + L''_1$, whereas Mitchell et al.[13] used $W + L_1$. Again increasing the temperature leads to the formation of a two-phase region 2Φ′, also consisting of two isotropic liquid solutions. The difference between 2Φ′ and 2Φ is that the lower (polymer-rich) phase shows a somewhat higher viscosity than in the 2Φ region and becomes permanent birefringent upon shearing the tube for a short time. In contrast to the $L_1 + L_3$ region, however, no flow birefringence occurs, which disappears after stopping the shear. With further increasing the temperature, the L_3 phase is formed for concentrations above 6 wt % PE6200, but now the one-phase temperature range is much larger than that in the concentrated region. After the transitions $L_3 \rightarrow L_3 + L_1 \rightarrow 2\Phi' \rightarrow L_2 + L_1$ again a two-phase region appears with two isotropic phases showing no birefringence under shear. In the whole phase diagram no three-phase regions could be detected.

The spongelike L_3 phase can be diluted down to 6 wt % Poloxamer, whereas the lamellar L_α phase only can be diluted down to 8 wt %. A similar trend has been found for a specially purified sample of $C_{12}EO_5$[19] that can form the L_3 phase at concentrations above ca. 0.5

wt %, whereas more than 1 wt % $C_{12}EO_5$ is needed to form the L_α phase. With further diluting the Poloxamer solutions, the continuous bilayer structure is ruptured and a dilute solution (presumably L_1) separates on the top from the concentrated Poloxamer solution. In the concentrated phase there are still bilayer fragments, which are too small to show spontaneous orientation and hence birefringence. But with shearing the sample for a short time they can be oriented and form a birefringent L_α phase. When these oriented samples are thermostated for several minutes (up to 1 h), the bottom L_α phase again is transformed to an isotropic phase.

Comparing the present phase diagram with cloud-point data from literature gives good agreement. Tiberg et al.[22] investigated the clouding behavior in the concentration range up to 10 wt %. For 10 wt % PE6200 they found a cloud point of CP ≈ 23 °C, which increases progressively with decreasing concentration until at 1 wt % CP is 30 °C. The complete phase diagram for PE6200 has been investigated by Wanka et al.[12] In the whole composition range they found an isotropic solution at temperatures below 40 °C. With increasing temperature a lamellar phase occurs over the concentration range 8–72 wt %. Further increase of the temperature leads to the formation of a multiphase region. This phase diagram differs somewhat from the more detailed cut presented here. Especially the two-phase region at lower temperatures has not been detected and the boundaries for the L_α phase are shifted somewhat to higher temperatures. Probably this may be attributed to batch variations with a varying content of hydrophobic contaminations.

Schmolka[23] reported CP for 1 wt % L62 ($EO_5PO_{30}EO_5$) to be 32 °C, whereas for 10 wt % L62 two cloud points are found at 24 °C and 40 °C. This phenomenon has been explained by contamination with hydrophobic block copolymer molecules, which precipitate at lower temperatures (24 °C) and are solubilized by the more hydrophilic compounds at increasing temperature, which by themselves show clouding at 40 °C. For L62 Ceresa[1] reported of a phase diagram for the concentration range 30–100 wt % and the temperature range 0–55 °C. Up to 70 wt % an isotropic solution is found for two temperatures, whereas at higher temperatures clouding occurs. Toward higher concentrations a "viscous paste" is formed, and beyond 80 wt % again a clear liquid phase occurs. Additionally in the polymer-rich corner a "cloudy viscous phase" appears at temperatures below 20 °C.

3.2. DSC. It is now well established that dilute aqueous solutions of Poloxamers show an endothermic DSC peak on heating.[3,12,24,25] With increasing temperature the equilibrium between polar and less polar (or even nonpolar) conformations in the PO chain is shifted to the latter one, which favors PO–PO interactions more than that between PO and water.[6] Consequently, the PO blocks are dehydrated and collapse to micelles. But also to detect transitions to lyotropic liquid crystalline phases, the DSC is a useful tool.[12] Figure 3 shows a DSC signal, which is typical for higher concentrations. The micellization process is represented as a broad peak, whose onset temperature can be described as the critical micellization temperature cmt. The transition from this L_1 phase to the lamellar phase L_α is illustrated by a sharp peak, which is followed by a broad tail. This peak shape is typical for Poloxamer phase transitions like $L_1 \rightarrow L_\alpha$ and $L_1 \rightarrow H_1$ (hexagonal).[12] At higher temperatures the transition $L_\alpha \rightarrow L_3$ appears as a well-defined peak, whereas the transition $L_3 \rightarrow L_1 + L_2$ is very broad. In Figure 4 the temperatures for the detectable phase transitions are summarized. Especially in the dilute region the phase boundaries are difficult to determine, as the peaks are very weak. But, in general, they show very good agreement with the optically determined phase diagram in Figure 2.

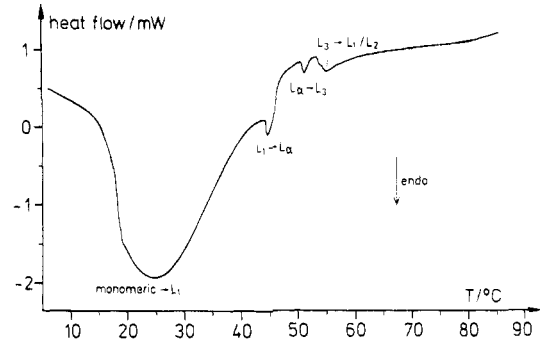

Figure 3. DSC signal for 30 wt % PE6200 with a heating rate of 0.2 K/min. L_1 = micellar solution, L_α = lamellar phase, L_3 = spongelike phase, L_1/L_2 = clouding.

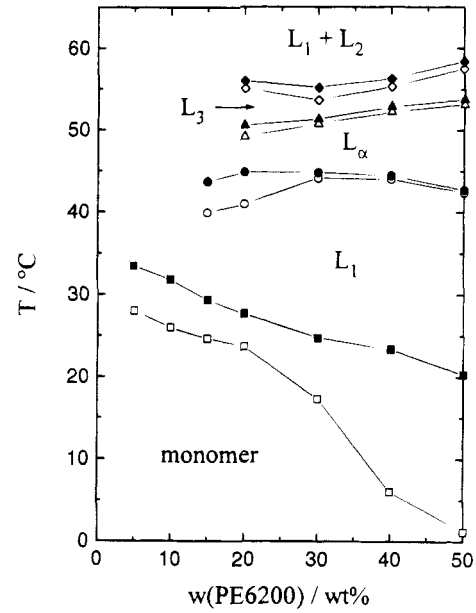

Figure 4. Phase transitions of aqueous PE6200 solutions as determined by DSC measurements and a heating rate of 0.2 K/min. Open symbols correspond to the peak onset and filled symbols to the peak minimum.

Table 1. Enthalpies for Different Phase Transitions of the Binary PE6200/Water System As Determined by DSC Measurements[a]

w(PE6200)/ (wt %)	ΔH/(J/g of PE6200)			
	mono → L_1	$L_1 \rightarrow L_\alpha$	$L_\alpha \rightarrow L_3$	$L_3 \rightarrow L_1/L_2$
5	63.6			
10	69.3			
15	67.2	0.57		
20	38.7	0.77	0.022	0.25
30	37.2	1.00	0.17	1.1
40	47.1	0.70	0.27	0.69
50	26.4	0.40	0.23	0.34

[a] Mono = monomeric Poloxamer solution, L_1 = micellar solution, L_α = lyotropic lamellar, L_3 = spongelike phase, L_1/L_2 = clouding.

In Table 1 a list of transition enthalpies for the different phases are shown. The micellization enthalpy is more than 2 orders of magnitude larger than the enthalpy for the formation of the L_3 phase. Interesting to note is that the enthalpies for the transitions $L_1 \rightarrow L_\alpha$ and $L_3 \rightarrow L_1/L_2$ are of similar quantity. As described above the broad micellization peak is due to dehydration of the PO blocks. In this context it is of interest that the formation of the L_α phase starts within this micel-

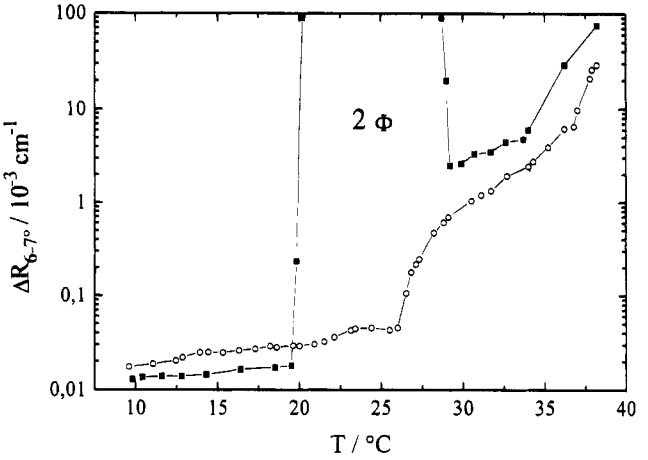

Figure 5. Light scattering of 15 wt % PE6200 as a function of temperature: (■) before filtration; (○) after filtration at 27.0 °C with a nominal filter pore size of 50 nm.

lization peak, hence when the dehydration process still takes place. In other words, the dehydration process directly influences the headgroup area, which is responsible for the formation of the lyotropic liquid crystalline phases.

Comparison of Figures 2 and 4 now gives an explanation of why the two-phase region 2Φ disappears with increasing temperature or increasing concentration. As found for many Poloxamers the cmt decreases with increasing concentration.[3,12,24,25] The same is found for PE6200, whose cmt follows the two-phase region 2Φ but decreases more strongly above 30 wt %. The minimum of the micellization peak is placed above 2Φ, i.e., when the turbid solutions get clear. The explanation for this behavior is as follows: At a constant Poloxamer concentration and low temperatures only monomeric PE6200 is present in solution. With increasing temperature the most hydrophobic compounds in the broad distribution of Poloxamer molecules separate from the solution; i.e., clouding occurs. Further increase of temperature now drives the more hydrophilic compounds to aggregate. These polymer micelles now solubilize the separated hydrophobic phase, and hence the solution gets clear again. This is in close analogy to the "anomalous association behavior" of L64 (or Poloxamer 184 = EO_{12}-$PO_{30}EO_{12}$) found by Zhou and Chu.[2] They showed that with increasing temperature the scattering of a L64 solution increases rapidly before the onset of micellization, whereas above the cmt it decreases again and then increases only slightly with temperature. This maximum, and thus the clouding behavior, disappears when the cloudy solutions are filtered through membranes with 50-nm pore size. Thereby, hydrophobic contaminations from synthesis are removed, which are responsible for this anomaly. This procedure also can be applied successfully in the present case, as described in the next chapter.

3.3. Purification. In close analogy to the purification of L64 described by Zhou and Chu,[2a] we will show below that this procedure also works for PE6200. Figure 5 shows the static light scattering of 15 wt % PE6200 as a function of temperature. Below 19.5 °C the scattered intensity is very low, which corresponds to the "unimer region". Between 20 and 29 °C clouding occurs and the intensity increases rapidly, corresponding to the "anomalous region". Above 29 °C the scattered intensity again decreases to a level 2−3 orders of magnitude higher than in the unimer region. For this "micelle region" aggregation numbers of several hundreds can be estimated, using the refractive index

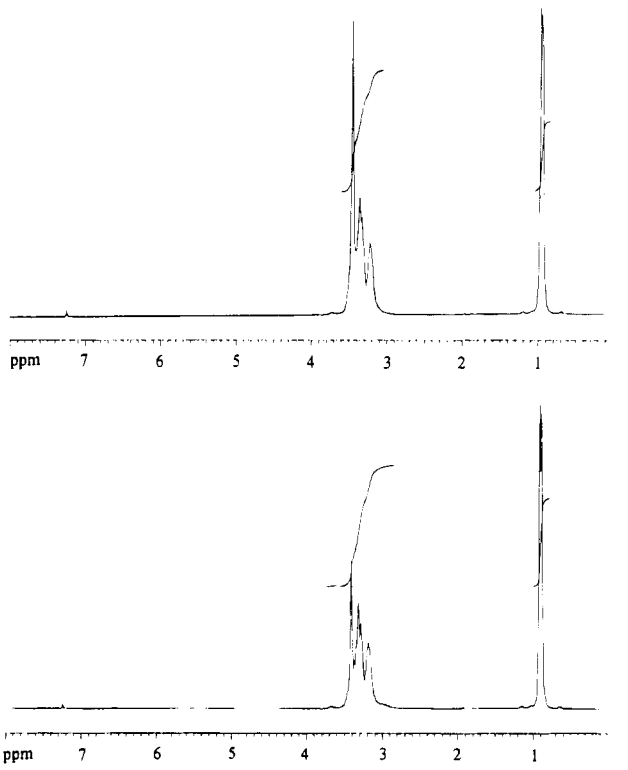

Figure 6. ^{1}H-NMR spectra of PE6200 at 20 °C in $CDCl_3$: (top) technical product; (bottom) hydrophobic fraction 2.

increments in ref 12 and a structure factor $S(q)$ of about 0.2. At temperatures above 34 °C the scattered intensity again increases, indicating the formation of large nonspherical, presumably ellipsoidal, aggregates.

One possibility to remove the hydrophobic contamination is the filtration experiment described by Zhou and Chu.[2a] A cloudy sample of 15 wt % PE6200 can be filtrated by a membrane with 50-nm pore size. Figure 5 shows that after filtration the two-phase region 2Φ indeed has disappeared. Now the normal temperature-driven micellization with cmt = 26.1 °C is observed in close analogy to Zhou and Chu.[2a] At higher temperatures, however, the scattered intensity, and therefore the mean aggregation number, is smaller after filtration. This may be explained by the loss of "solubilized" hydrophobic contaminants, which swell up the micelles. Now the mean aggregation numbers are in the region between 30 and 100. Filtration with a pore size of 100 nm failed, as the clear filtrate got cloudy again after thermostating.

Another way to remove the hydrophobic contaminants is to thermostate a cloudy 15 wt % solution at 27.0 °C, a temperature above the cloud point of CP = 22.0 °C but below the peak minimum in the DSC experiment (T_{min} = 29.3 °C). Although this temperature lies above the cmt = 24.6 °C, it has been chosen to allow phase separation within a reasonable time. After several days two phases separate with an upper bulk phase Φ_1 and a small viscous phase Φ_2 on the bottom of the tube. Freeze drying under vacuum gives two viscous block copolymer samples named fraction 1 for the hydrophilic compound (Φ_1) and fraction 2 for the hydrophobic contamination (Φ_2).

To analyze the composition of the block copolymer samples, ^{1}H-NMR spectra in $CDCl_3$ were made. In Figure 6 the spectra of the technical product and the hydrophobic fraction 2 are compared. The doublet at 0.9 ppm corresponds to the methyl groups of the PO block, and the signal between 3.0 and 3.4 ppm refers to

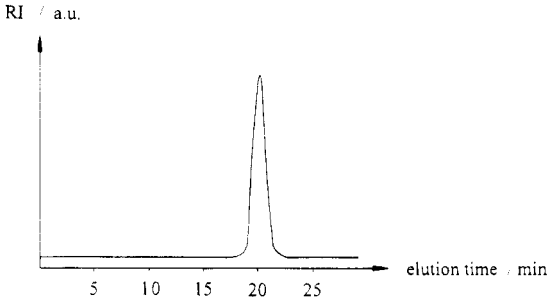

Figure 7. Gel permeation chromatogram of the technical product PE6200 dissolved in $CHCl_3$, at $T = 30$ °C and with refractive index detection.

Table 2. Composition of PE6200 before and after Fractionation at 27.0 °C As Derived by ^1H NMR

	wt % EO
technical product	29.5
hydrophilic fraction 1	29.9
hydrophobic fraction 2	17.8

the methylene protons in both the EO and the PO blocks. Close to the procedure reported in ref 2a, the composition of the samples are calculated and summarized in Table 2. After fractionation the EO content of the hydrophilic major component (fraction 1) is only slightly higher than that of the technical product. The EO content of the hydrophobic fraction 2, however, has decreased to almost half that of the technical product. This may be an indication for a hydrophobic EO_xPO_y diblock contamination.

To check this, GPC experiments were made to analyze the particle size distribution of the different samples. ABA triblock copolymers contaminated with AB diblock copolymer should show two GPC signals or at least a shoulder at the low molecular weight side of the main peak. This behavior can be found for F127 ($EO_{97}PO_{69}EO_{97}$), which contains about 10% "impurities".[26] Due to its high EO content, however, F127 does not show any anomalous association behavior. In Figure 7 the GPC signal of the technical product is shown. Only one well-defined peak can be observed indicating a relatively monodisperse distribution of molecular weights. After fractionation the hydrophilic compound 1 and the hydrophobic compound 2 show similar curve shape, but at slightly different elution volumes. As the column is calibrated for polystyrene, absolute values for the molecular weight cannot be calculated. From the relative position of the peak maximum, however, we can conclude that the molecular weight of the hydrophilic compound is somewhat higher than that of the original sample and the MW of the hydrophobic compound is somewhat smaller than that of the technical product.

Thus the results from GPC seem to contradict the conclusions from ^1H NMR. How can this be explained? In the GPC experiment different volumes of the polymer molecules are the reason why they can be separated. The smaller this difference, the more unlikely their resolution. In the present case the diblock copolymer EO_xPO_y differs from the triblock copolymer $EO_xPO_yEO_x$ only by a mass of about 260 (i.e., 10% of the total molar mass). Under the experimental conditions used here this difference seems to be too low to be detected.

Now we want to analyze the effect of the hydrophobic impurity on the phase behavior of PE6200. In Figure 8 the DSC signal of two samples of 30 wt % PE6200 are compared. As can be clearly seen, the phase behavior before and after filtration is essentially the same. Only the micellization peak has become much

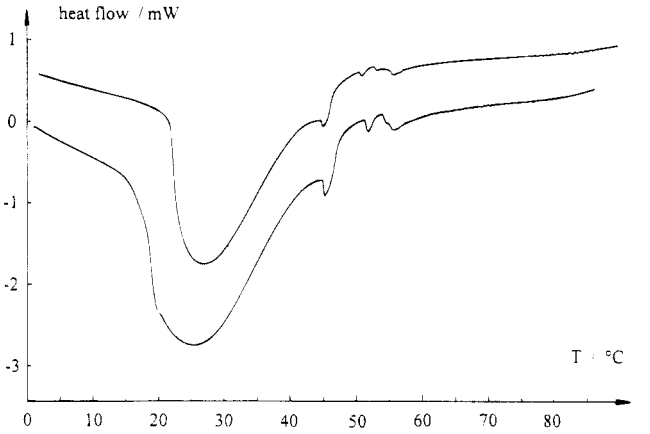

Figure 8. DSC signal of 30 wt % PE6200: (bottom) before filtration; (top) after filtration at 19.0 °C with 50-nm pore size. Phase transitions are as described in Figure 3.

sharper after removing the contamination. Similar conclusions can be drawn for 15 wt % PE6200 before and after filtration, where the micellization peak also gets sharper (results not shown).

As the hydrophobic contamination does not influence the phase behavior of PE6200 (except the formation of the 2Φ region), all investigations were made with the technical sample without fractionation. As described above, removal of the hydrophobic fraction may shift the phase boundaries by 1−2 °C but will not affect the existence of the L_α and L_3 phases, which are of particular interest in this investigation.

3.4. Influence of Salt. As reported previously,[24,27−30] additives like salt and surfactants strongly influence the phase behavior of Poloxamers. Salts like LiCl, NaCl, and KCl decrease the cmt of Poloxamers linearly with increasing electrolyte concentration. The same influence is found for the gelation process, where the gelation temperature decreases linearly with increasing salt concentration.[28,30] In the following we show that this linear decrease of the transition temperatures with increasing salt concentration also is valid for the L_α and L_3 phases. In Figure 9 the phase transitions of a 30 wt % PE6200 solution are plotted against the concentration of NaCl. As can be clearly seen, all phase transitions are shifted linearly to lower temperatures when the salt concentration is increased. The slope dT/dw is 3.57 ± 0.26 °C/wt %, which corresponds to 20.9 ± 1.5 °C·(L/mol). This value is comparable to that obtained for the decrease of CP for F127 ($EO_{97}PO_{69}EO_{97}$) and L64 ($EO_{12}PO_{30}EO_{12}$), which are determined to be 44[30] and 13 °C·(L/mol).[27]

In general, the phase behavior of Poloxamers depends on the presence of hydration water for the EO and PO blocks. Addition of salt binds increasing amounts of water, which also has to be desorbed from the Poloxamer molecules. Due to this competition for hydration water, the PO blocks now become more hydrophobic and induce micellization at lower temperatures than without salt. As the slope for all phase transitions investigated remains the same, a similar mechanism seems to be responsible for this phenomenon.

3.5. SANS. In this chapter SANS is used to investigate the different phase transitions of PE6200 induced by increasing temperature. We focused our interest on the appearence of the L_α and L_3 phases, and the results are more or less qualitative. Quantitative evaluation will be reserved for a forthcoming paper.

Figures 10−12 show the scattering function of respectively 10%, 30%, and 50% PE6200 solutions in D_2O,

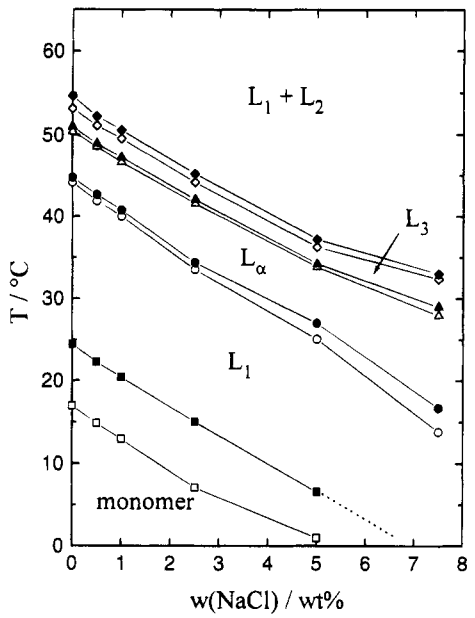

Figure 9. Transition temperatures of 30 wt % PE6200 as a function of the concentration of NaCl, determined by DSC measurements and a heating rate of 0.2 K/min. Open symbols correspond to the peak onset and filled symbols to the peak minimum.

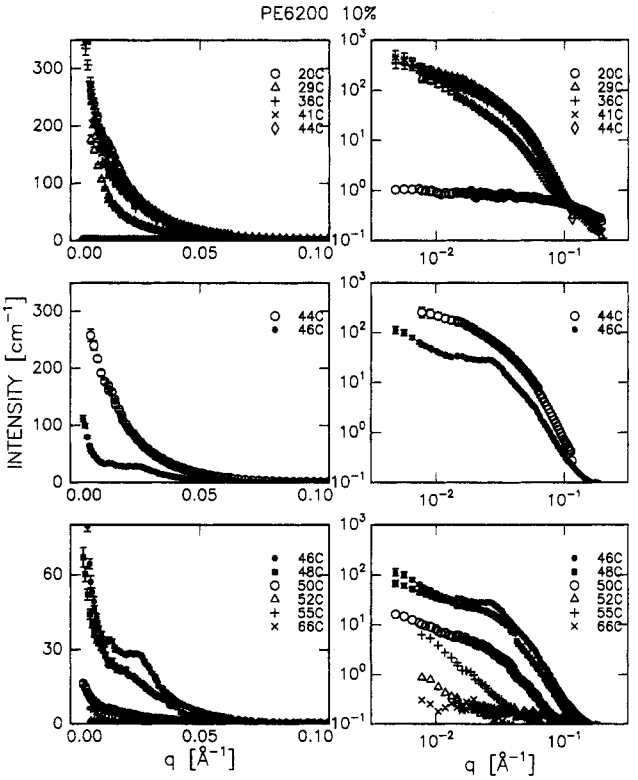

Figure 10. Scattering function of 10 wt % PE6200 (top) T = 20–44 °C (unimer phase and mixed phase); (middle) T = 44 °C (L_α) and T = 46 °C (L_3); (bottom) T = 46–66 °C (L_3 and mixed phases).

as obtained at the 18–65 °C temperature range. The scattering function shows dramatic nonmonotonic temperature and concentration dependencies with highest intensity within the 30–55 °C regime, roughly. In an attempt to make the individual regimes more clear, we have divided the experimental data into three figures covering different temperature intervals. At the lowest temperatures, as well as at the highest, the intensity is markedly reduced. The scattering function thus clearly evolves through the various phases which were

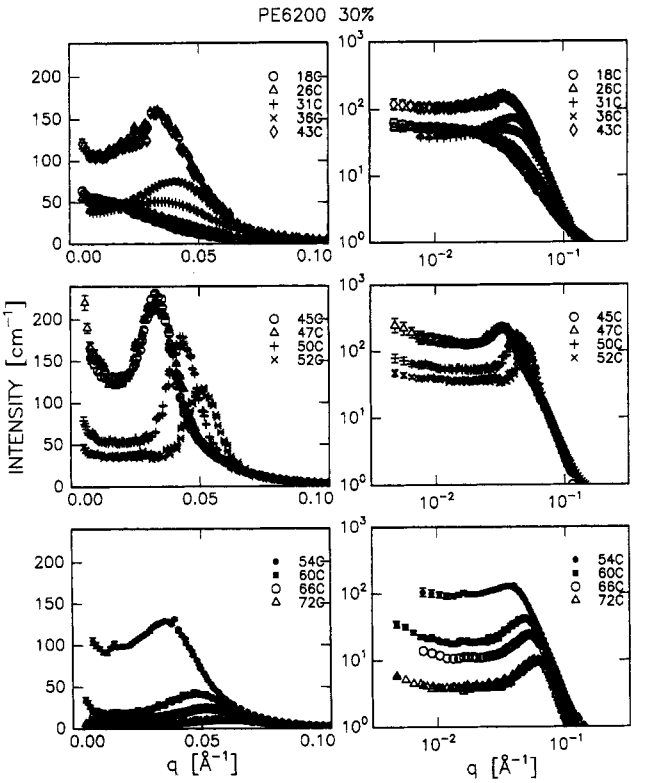

Figure 11. Scattering function of 30 wt % PE6200; (top) T = 18–36 °C (L_1 phase); (middle) T = 43–52 °C (L_α); (bottom) T = 54–72 °C (L_3 and mixed phases).

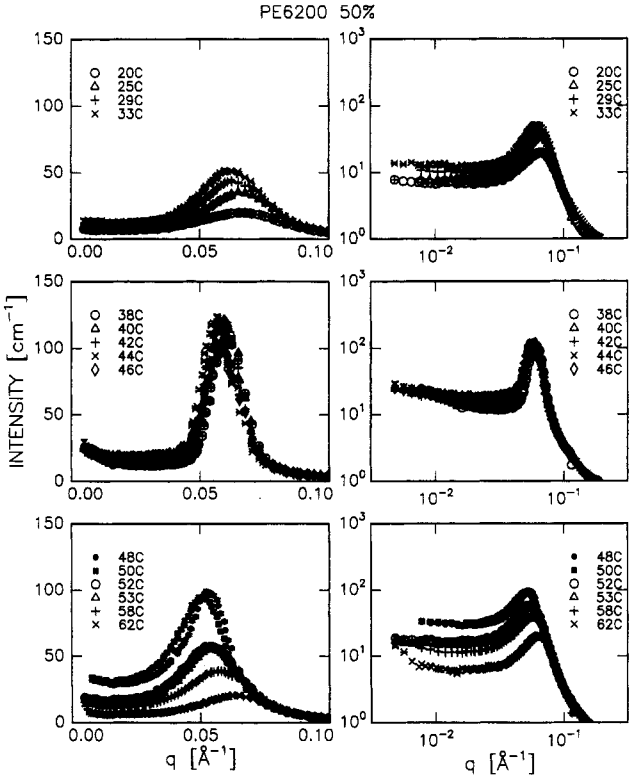

Figure 12. Scattering function of 50 wt % PE6200: (top) T = 20–33 °C (L_1 phase); (middle) T = 38–46 °C (L_α); (bottom) T = 48–62 °C (L_3 and mixed phases).

observed in other techniques: calorimetry, light scattering, and conductivity, as presented in this paper.

The kinetics of phase separation is rather slow, so that at the phase boundaries an emulsion of two phases is in the neutron beam. Hence, the scattering pattern shows smooth transitions with increasing temperature due to superposition of two spectra.

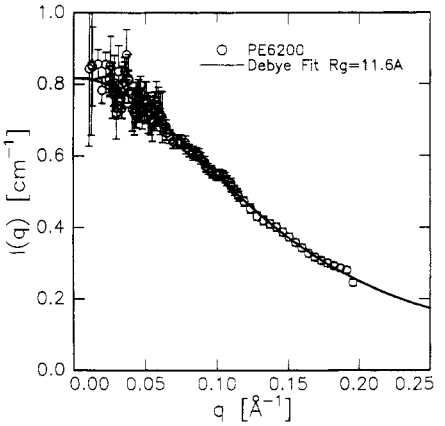

Figure 13. Scattering function of 10 wt % PE6200 at 18 °C. The solid line is a least-square residual fit to the Debye function, giving R_g = 12 Å.

In Figure 13, we show fits to simple Gaussian line shape. Although the peaks clearly are non-Gaussian, such fits, when restricted to the q-regime near the maximum intensity, give a well-defined indication of the different high-temperature phases and phase transitions. The transition temperatures agree well with the values obtained from independent studies. The small discrepancies may be associated with the limited time for thermodynamic stabilization in the scattering experiment.

Unimers. Within the low-concentration, low-temperature window (exemplified by the data set of a 10% sample at 20 °C displayed in Figure 10) the scattering function shows low intensity, revealing that the polymers are dissolved as unimers. The scattering function follows quite well the Debye function:

$$I(q) \sim x^{-2}(e^{-x} + x - 1) \quad (4)$$

where $x = (qR_g)^2$, R_g being the polymer radius of gyration. Fit to this formula gives the polymer radius of gyration, R_g = 12 Å. For comparison, we found R_g = 17 Å for the equivalent copolymer $EO_{25}PO_{40}EO_{25}$ (P85)[31] and R_g = 22 Å for $EO_{99}PO_{65}EO_{99}$ (F127),[32] thus showing some deviation from the expected $R_g \propto \sqrt{N}$ relationship for Gaussian chains. Moreover, the obtained R_g values are relatively small, perhaps indicating that the most hydrophobic part (PPO block) is more compact than simple Gaussian.

L_1 Phase. As the temperature is increased, the scattering intensity increases, revealing association of the copolymers into aggregates, presumably in the form of micelles. The $I(q)$ function shows, however, a significant difference from the form of spherical micelles dominated by a dense core, as seen for other Poloxamer micelles.[31] The actual form of these micelles needs further investigations.

At higher temperatures, interparticle correlations become significant, as seen in the developments of a pronounced correlation peak. Within the whole regime assigned as L_1 (basically given by the top figures), the $I(q)$ function changes significantly with temperature within the whole q range measured, indicating major temperature-dependent changes not only in the intermicellar correlations but also in the structure of the individual aggregate. The exact form of these L_1 phase aggregates will be studied further in an upcoming investigation.

L_α Phase. The scattering function changes markedly its character going from the L_1 phase to the L_α phase: first of all, the correlation peak becomes significantly more narrow. This is seen in Figure 14, which shows the peak position and peak width when fitted to a Gaussian in a relatively narrow regime close to q_1.

In a relatively narrow temperature regime close to 50 °C, the scattering function shows the characteristics typical for a dilute lamellar L_α phase:[20,33] a narrow first-order peak at q_1 and a weak shoulder indicating the second-order reflection and significant small-angle scattering.

In the lamellar phase, the peak position changes significantly by temperature. This is in particular the situation for the low-concentration sample (30%) and less for the higher concentration (50%). In Figure 15 the concentration-dependent lamellar periodicity is shown, as obtained from $d = 2\pi/q_1$ (q_1 values given in Figure 14). It is seen that the lamellar q_1 value increases roughly linearly with polymer concentration at the entrance to the L_α phase (marked as low T). This is as expected for ideal one-dimensional swelling:

$$d = \delta/\Phi \quad (5)$$

assuming conservation of volume and constant bilayer thickness δ. Φ is the polymer volume fraction. A least-squares fit to this equation gives the bilayer thickness $\delta \approx 55$ Å. The corresponding length of the fully extended PO block in "zigzag" and "meander" configurations would be 130 and 72 Å with monomer lengths of 3.6 and 2.0 Å,[2] respectively. Comparing to the polymer radius of gyration found in the unimer phase (see above), R_g = 12 Å, this indicates highly stretched copolymers in the L_α phase.

In principle, the lamellae structure can have monolayer or bilayer structure. In the case of monolayers the PO block is more or less stretched, forming the hydrophobic layer. On both sides of the layer the EO blocks protrude into the aqueous phase. In the case of bilayers the PO block is U-shaped and both EO groups protrude only at one side into the aqueous phase. In both cases the lamellar thickness δ is determined by the length of the PO block and correspondingly is limited by the maximum extension of the chain. For both structures δ will be approximately the same so that we cannot decide between them with the above results.

At higher temperatures the lamellar periodicity is dramatically reduced, approaching that of the high concentration d value, basically independent of Φ. This may indicate that excess water is expelled from the bilayers as the temperature is increased. An alternative explanation of the large temperature dependence could be related to the flexibility of the bilayers, thus being more flexible near the L_1 phase (larger periodicity) and less at higher temperatures.

L_3 Phase. While the first-order peak position q_1 of the L_α phase increases with temperature, we observe a marked (discontinuous) drop in the position of maximum intensity, q_{max}, when crossing into the L_3 phase. The scattering function changes in character to a form also seen in the L_3 phase of low molecular complex fluids.[19,20] The change from L_α to L_3 character is perhaps better seen in the example displayed in Figure 16, where we have shown the L_α and L_3 scattering functions for a 30% solution.

Since the peak position changes markedly within both phases, there is no single ratio of the characteristic peak values. A well-defined unique value of this ratio could be given by the values approaching either side of the phase-transition temperature. For the 20%, 30%, and 40% samples (results for 20% and 40% not shown), we find that this ratio q_1/q_{max} is 1.5, whereas the 50%

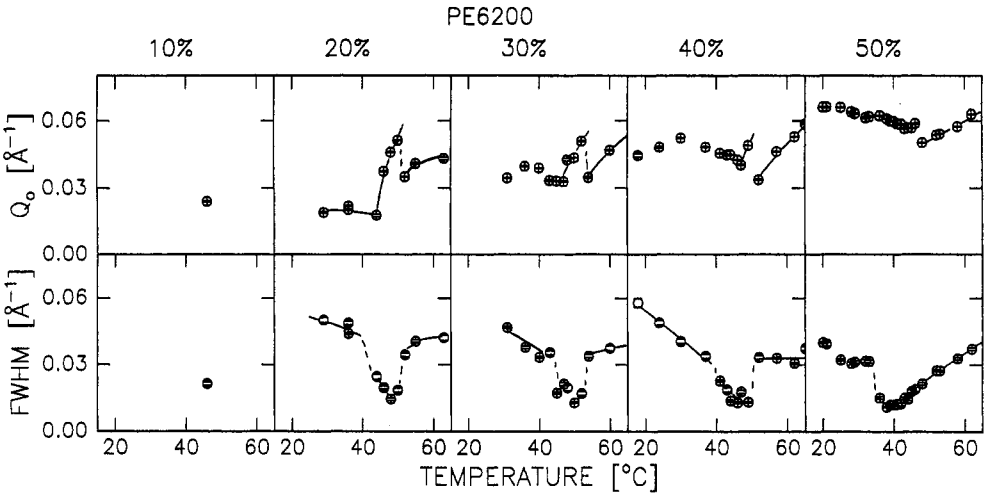

Figure 14. Peak position and peak width versus temperature of PE6200 as obtained from fits to Gaussian line shape.

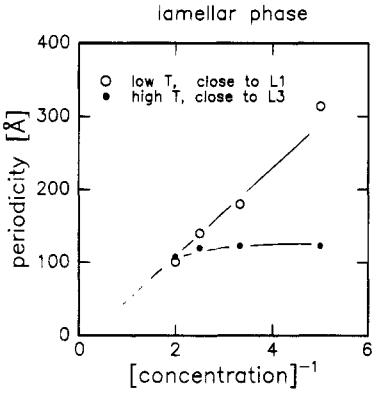

Figure 15. Lamellar repeat distance versus polymer concentration of PE6200 in D_2O. Open symbols represent the values at the low-temperature limit of the L_α phase, while closed symbols give the values at the high-temperature limit.

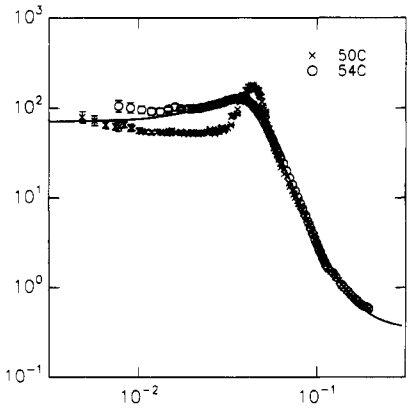

Figure 16. Scattering function of 30 wt % PE6200 at $T = 50$ °C (L_α) and $T = 54$ °C (L_3). The solid line represents the best fit to the Teubner–Strey function.

sample has the ratio 1.3. Milner et al. predicts actually a ratio of 1.5 according to a cubic tesselation model.[34]

The structure factor of the L_3 phase has been approached by several authors. For example, Gompper et al. have given a detailed analytical formula for the scattering function.[35] Even though their formula has rather many independent parameters to fit, we have not been able to get satisfactory agreement with our experimental data. For example, Gompper et al. find a $I \propto q^{-2}$ relationship at high-q values, while our data have a much more steep q dependence. The more simple Teubner–Strey model[36] gives better agreement with the

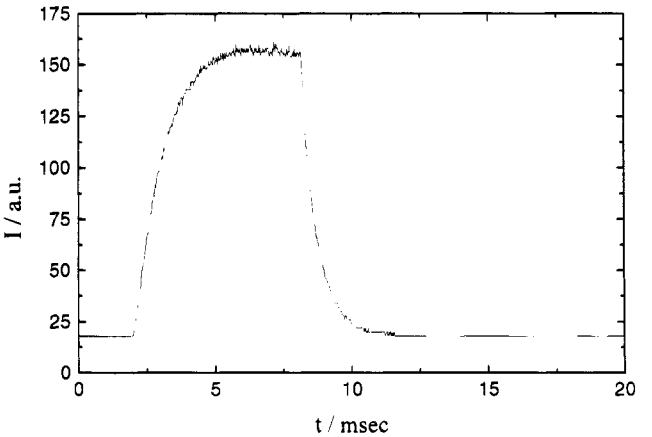

Figure 17. Electric birefringence signal for 15 wt % PE6200 in the L_3 phase ($U = 350$ V, $d = 5.5$ mm, $T = 48.7$ °C). The monoexponential decay can be fitted by the parameters $\tau_R = 2.3$ ms and $\alpha = 0.92$.

experimental data but cannot describe the low-q intensity. The solid line in Figure 16 is a best fit to the Teubner–Strey model, including an incoherent background and instrumental smearing effects. More details on the L_3 scattering function are in progress and will be published elsewhere.

Upon further heating within the L_3 phase and into the two-phase L_1/L_2 regime, the peak position changes continuously to larger values.

3.6. Electric Birefringence. To give evidence for the spongelike L_3 phase in the system PE6200/water, different techniques were used, which have been found suitable in the cases of $C_{12}EO_5$/water[19,20] and C_{14}DMAO/C_nOH/water.[17] For each PE6200 concentration the temperature in the middle of the L_3 region has been selected, so that the temperature for the measurements increases with increasing Poloxamer concentration.

PE6200 solutions in the L_3 phase show a marked signal in the electric birefingence measurement (Figure 17). At each concentration the sign of the signal Δn is positive. The rise time after switching on the electric field and the decay time after switching off are the same, indicating that no permanent dipole moments are present. The decay can be fitted by a stretched monoexponential function rather than with a pure monoexponential function ($\alpha = 1$):

$$I(t) = I_0 + A \exp(-t/\tau_R)^\alpha \qquad (6)$$

The exponent $\alpha < 1$ may be a result of the polydispersity of the block lengths and hence a consequence of

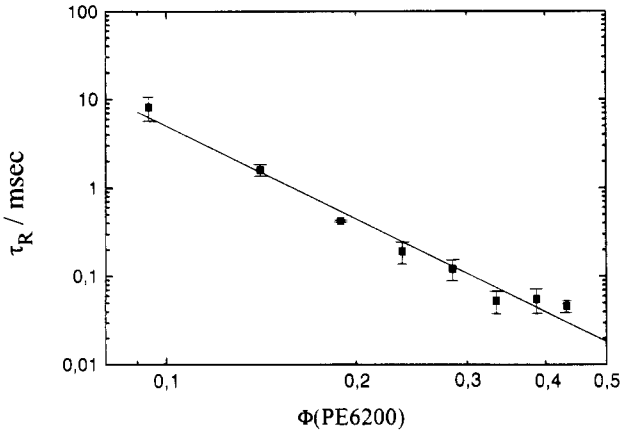

Figure 18. Orientational relaxation time τ_R of binary PE6200/water solutions in the L_3 phase as determined from the stretched monoexponential fit of the electric birefringence signal; $\alpha = 0.7-0.9$, experimental temperature in the middle of the L_3 region.

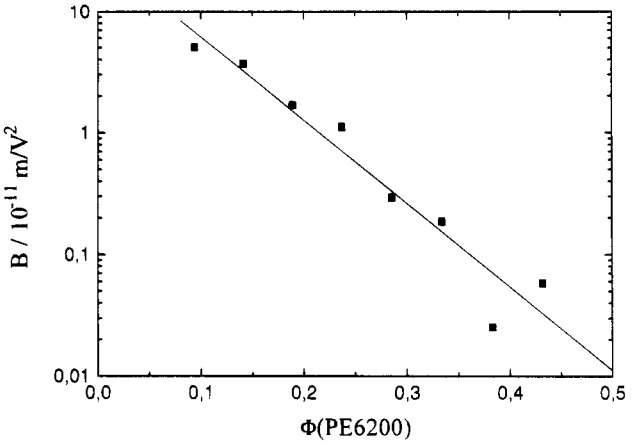

Figure 19. Kerr constant of PE6200 solutions in the L_3 phase as a function of the volume fraction; experimental temperature in the middle of the L_3 region.

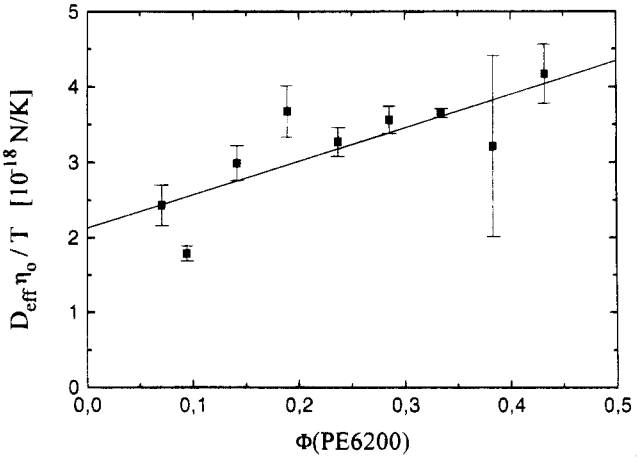

Figure 20. Reduced cooperative diffusion coefficient of PE6200 in the L_3 phase; experimental temperature in the middle of the L_3 region.

inhomogeneities in the bilayer thickness. The orientational relaxation time τ_R depends strongly on the volume fraction of the bilayer structure and decreases with increasing Poloxamer concentration (Figure 18). In a double-logarithmic plot of τ_R as a function of the volume fraction of PE6200, a linear dependence can be found with a slope of -3.5 ± 0.2. Miller et al.[17] found the slope for τ_R as a function of Φ to be -3.02 for the L_3 phase in the system C_{14}DMAO/1-hexanol/water. They took this as an indication for the orientation of platelike micelles, as theory predicts a slope of -3 for disklike aggregates. Porte et al.[37] found that also for the L_3 phase τ_R scales with Φ^{-3}, although both structures are completely different. From τ_R they obtain the persistence length ζ_H by

$$\frac{1}{\tau_R} = \frac{6kT}{3\pi\eta\zeta_H^3} \tag{7}$$

with k as Boltzmann's constant, T as the absolute temperature, and η as solvent viscosity.[37]

With increasing Poloxamer concentration not only the relaxation time but also the birefringence decreases. As a measure for the electric birefringence the Kerr constant B can be used, which is defined by:

$$B = \lim_{E\to 0} \frac{\Delta n}{E^2\lambda} \tag{8}$$

with Δn as the birefringence, E as the electric field, and λ as the wavelength of the laser. In Figure 19 the Kerr constant B is plotted as a function of the PE6200 concentration. B decreases exponentially with increasing concentration, so that at 50 wt % only a very weak signal is detectable. This is in contrast to the predicted scaling law $B \sim \Phi^{-1}$.[37] But also for the system *n*-dodecylbetaine/pentanol/water, a deviation from this Φ^{-1} relation is found and B has to be renormalized by a logarithmic correction.[37] The decrease of τ_R and B with increasing concentration may be a result of increasing curvature of the bilayers. At low concentrations the mesh size of the bicontinuous structure has to be relatively large in order to occupy the whole sample volume. The persistence length is large, which gives rise to a strong signal in electric birefringence measurements and a long orientational relaxation time. With increasing volume fraction of Poloxamer the mesh size decreases in order to fill the whole volume. The persistence length decreases in size, which leads to a decrease of the birefringence signal and the orientational relaxation time τ_R.

3.7. Dynamic Light Scattering. For the same concentration series as in 3.6 dynamic light scattering measurements were made to obtain the cooperative diffusion coefficient in the L_3 phase. To take the increasing temperature and hence the decreasing solvent viscosity[38] into account, the reduced effective diffusion coefficient $D_{eff}\eta_0/T$ instead of D_{eff} has been plotted as a function of the PE6200 concentration (Figure 20). As can be seen, $D_{eff}{}^*\eta_0/T$ increases linearly with increasing Poloxamer volume fraction. Extrapolation to $c = 0$ gives a value of $2.11 \pm 0.35 \times 10^{-18}$ N/K for the reduced diffusion coefficient of the L_3 phase at infinite dilution. This is in contrast to the behavior of hydrocarbon surfactants. As predicted by theory[37] and found experimentally,[17,37] D_{eff} increases linearly with Φ and approaches zero at infinite dilution. From the diffusion coefficient a hydrodynamic length ζ_h can be obtained using the Stokes–Einstein equation:

$$D_{eff} = \frac{kT}{6\pi\eta\zeta_h S(q)} \tag{9}$$

Applying eq 9 to the extrapolated value and assuming that at infinite dilution the structure factor $S(q)$ is unity, we obtain a hydrodynamic length of $\zeta_h = 344 \pm 102$ nm. In the next chapter the dimensions in the L_3 phase are summarized as derived by different methods.

3.8. Dimensions in the L_3 Phase. In Figure 21 the results of dynamic light scattering, electric birefrin-

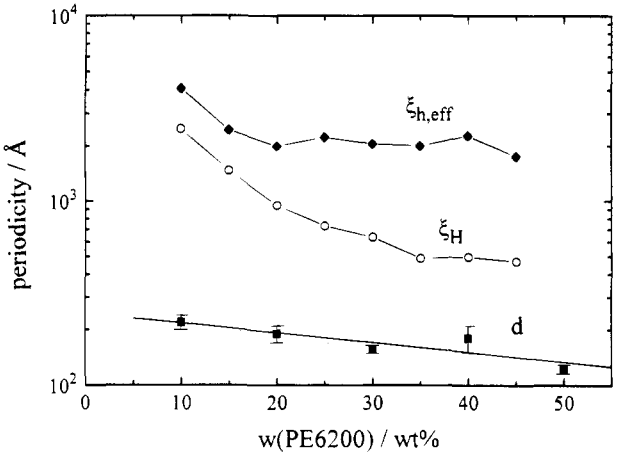

Figure 21. Dimensions in the L_3 phase of PE6200: d from q_{max} in SANS measurements, ζ_H from electric birefringence, and $\zeta_{h,eff} = \zeta_h S(q)$ from dynamic light scattering.

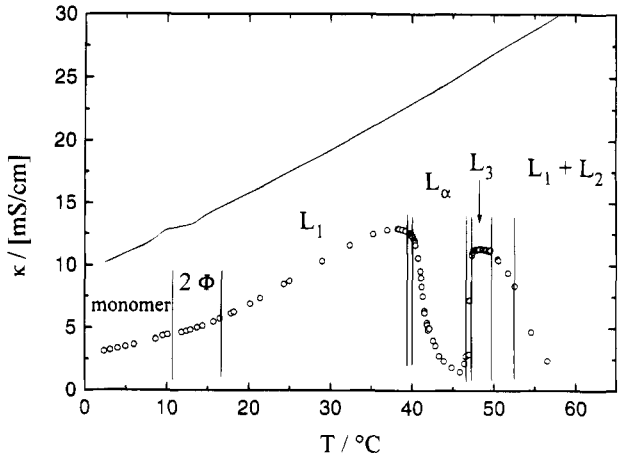

Figure 22. Specific conductivity of 1 wt % (≅0.17 mol/L) NaCl in the absence (—) and in the presence (○) of 30 wt % PE6200. Additionally, the phase boundaries of 30 wt % PE6200 + 1 wt % NaCl are shown.

gence, and SANS for the periodicity in the L_3 phase are summarized. With increasing polymer concentration, the dimensions within the L_3 phase decrease. As the different techniques characterize distinct parts of the sponge structure, the scales differ significantly. The lamellar distance d from SANS describes the spacing between two neighboring lamellae and hence has the smallest dimension. The relaxation in electric birefringence experiments corresponds to the deorientation of disklike structures in the lamellar interface (presumably that in the saddle-point region). As these structures are large compared to the lamellar distance (Figure 1), the persistence length ζ_H is much larger than d. With increasing polymer volume fraction the disklike structures in the bicontinuous lamellae decrease; hence, ζ_H approaches d for high concentrations.

The effective hydrodynamic length $\zeta_{h,eff}$ from dynamic light scattering, however, describes the cooperative diffusion. The structure factor $S(q)$ certainly is much smaller than 1; therefore, ζ_h has to be even larger as shown in Figure 21. As $\zeta_{h,eff}$ is by a factor of 2–4 higher than ζ_H from electric birefringence, the cooperative diffusion includes larger segments of the sponge structure than the rotation of disklike parts of the lamellae.

3.9. Specific Conductivity. The electrical conductivity of electrolyte in nonionic surfactant solutions strongly depends on the phase behavior of the surfactant.[19] In general, the specific conductivity κ of electrolyte solutions in the presence of surfactant or polymer is lower than in the pure electrolyte solution.[39] This is due to partial binding of ions to micellar or liquid crystalline aggregates; thus, the electrolyte volume fraction decreases. But more important for the lower conductivity is the obstruction effect, which lengthens the effective paths of moving ions. In the case of liquid crystalline phases the lower conductivity of surfactant/electrolyte mixtures additionally is effected by isolating the electrolyte solution from the bulk solution by lyotropic structures like lamellae.

In Figure 22 the specific conductivity of 1 wt % (≅0.17 mol/L) NaCl is shown as a function of temperature. κ_0 increases linearly with increasing temperature. In the presence of 30 wt % PE6200 the conductivity κ now is much lower than κ_0 due to the higher viscosity of the solution (increase by a factor of 10) but increases also with temperature. With reaching the L_α phase κ decreases strongly (down to 6% of κ_0), indicating isolated lamellar structures, which are not connected to the bulk solution. With transition to the L_3 phase κ again increases, but to a level below that of the micellar L_1 phase (43% of κ_0). The bicontinuous spongelike structure of the L_3 phase facilitates the migration of ions, rather than the plain lamellar structure of the L_α phase. The experimentally determined value $\kappa/\kappa_0 = 0.43$ for the L_3 phase is lower than $^2/_3$, as predicted by theory.[14,40] This may be due to the nature of the Poloxamer "headgroup". In contrast to hydrocarbon surfactants with small well-defined headgroups, Poloxamer headgroups are EO blocks with a relatively broad length distribution. The longer blocks may reach deeper into the aqueous channels and thereby increase the obstruction effect by hindering the ion transport. A more pronounced deviation from the theoretical value of $^1/_3$[40] is found for the L_α phase with $\kappa/\kappa_0 = 0.06$. This means that the lamellar structure is not really bicontinuous but separated by defects into smaller subvolumes. This hinders the migration of ions and therefore reduces the conductivity more than predicted for flat infinite lamellae.

At temperatures above 50 °C κ decreases again, which is caused by spontaneous phase separation. The lower polymer-rich phase shows very low conductivity, whereas the upper water-rich shows higher conductivity than κ_0, because NaCl is enriched in this phase. It is interesting to note that the two-phase region $L_1 + L_2$ can be detected by specific conductivity, while the region 2Φ shows no change in κ.

4. Conclusions

We investigated the phase behavior of PE6200 (EO_6-$PO_{36}EO_6$) in more detail as in previous studies. We found some analogies to the phase behavior of nonionic surfactants of the type C_nEO_x. For the first time the spongelike L_3 phase has been found in binary Poloxamer/water systems, which usually is found in more complex surfactant/cosurfactant/water systems. The L_3 phase region lies directly above the lamellar phase L_α but can be more diluted than the L_α phase. Evidence for the L_3 phase has been given by SANS, DSC, electric birefringence, dynamic light scattering, and conductivity measurements, which have been proven as useful tools to characterize the bicontinuous structure. In principle, the Poloxamer lamellae can be formed by monolayers or bilayers of triblock copolymers, as shown in Figure 23. In the case of monolayers, the PO block is more or less stretched, forming the hydrophobic layer. On both sides of the layer the EO blocks protrude into the aqueous phase. In the case of bilayers the PO block is U-shaped, and both EO blocks protrude only at one side

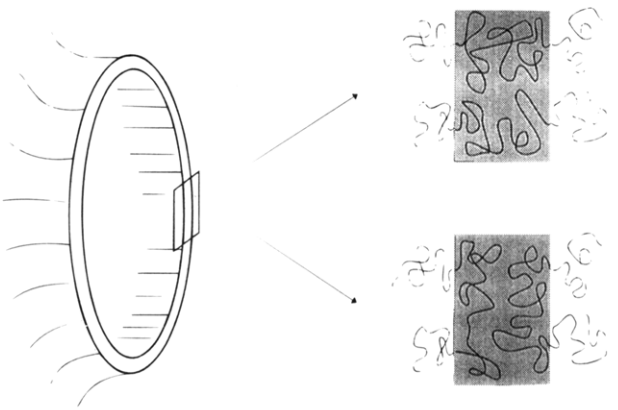

Figure 23. Model for monolayer (top) and bilayer (bottom) structures of a Poloxamer lamella.

into the aqueous phase. For the bilayer structure the adsorption/desorption process of monomeric Poloxamer is easier than in the monolayer structure. If a monomer wants to leave the monolayer, one hydrophilic EO block has to pass the hydrophobic PO layer, which is energetically unfavored.

Hence, for entropical reasons the bilayer structure of the lamellae seems to be more likely, but the monolayer structure cannot be ruled out completely. Nevertheless, the interface between the hydrophobic PO layer and the hydrated EO blocks is not expected to be sharply defined like for small hydrocarbon surfactants, as in Poloxamer micelles the segment density of the PO and EO units at the interface will show a smooth transition.

A method has been described to remove hydrophobic contaminations, which cause clouding at ambient temperatures. It has been shown that technical PE6200 contains about 10 wt % hydrophobic compounds, which only marginally influence the boundaries of the L_α and L_3 phases.

Acknowledgment. Christine Thunig is gratefully acknowledged for helpful discussions dealing with the phase diagrams and Claudia Schmidt for her help in NMR measurements. This work was supported by the DFG (SFB 213) and the Fonds der chemischen Industrie as well as by the Danish Natural Science Research Councils and the EU-Large Installation Program.

References and Notes

(1) Ceresa, R. *Block* and *Graft Copolymerization*; John Wiley & Sons: London, 1976; Vol. 2.
(2) (a) Zhou, Z.; Chu, B. *Macromolecules* **1988**, *21*, 2548. (b) Zhou, Z.; Chu, B. *J. Colloid Interface Sci.* **1988**, *126*, 171.
(3) Wanka, G.; Hoffmann, H.; Ulbricht, W. *Colloid Polym. Sci.* **1990**, *268*, 101.
(4) Brown, W.; Schillén, K.; Hvidt, S. *J. Phys. Chem.* **1992**, *96*, 6038.
(5) Yu, G.; Deng, Y.; Dalton, S.; Wang, Q.-G.; Attwood, D.; Price, C.; Booth, C. *J. Chem. Soc., Faraday Trans.* **1992**, *88*, 2537.
(6) Linse, P.; Malmsten, M. *Macromolecules* **1992**, *25*, 5434.
(7) Mortensen, K. *Europhys. Lett.* **1992**, *19*, 599.
(8) Mortensen, K. *Prog. Colloid Polym. Sci.* **1993**, *93*, 72.
(9) Mortensen, K.; Brown, W. *Macromolecules* **1993**, *26*, 4128.
(10) Alexandridis, P.; Holzwarth, J. F.; Hatton, T. A. *Macromolecules* **1994**, *27*, 2414.
(11) Alexandridis, P.; Athanassiou, V.; Fukuda, S.; Hatton, T. A. *Langmuir* **1994**, *10*, 2604.
(12) Wanka, G.; Hoffmann, H.; Ulbricht, W. *Macromolecules* **1994**, *27*, 4145.
(13) Mitchell, D. J.; Tiddy, G. J. T.; Waring, L.; Bostock, T.; McDonald, M. P. *J. Chem. Soc., Faraday Trans. 1* **1983**, *79*, 975.
(14) Porte, G.; Marignan, J.; Bassereau, P.; May, R. *J. Phys. (Fr.)* **1988**, *49*, 511.
(15) Anderson, D.; Wennerström, H.; Olsson, U. *J. Phys. Chem.* **1989**, *93*, 4243.
(16) Skouri, M.; Marignan, J.; Appell, J.; Porte, G. *J. Phys. II (Fr.)* **1991**, *1*, 1121.
(17) Miller, C. A.; Gradzielski, M.; Hoffmann, H.; Krämer, U.; Thunig, C. *Prog. Colloid Polym. Sci.* **1991**, *84*, 243.
(18) Hoffmann, H.; Thunig, C.; Munkert, U.; Meyer, H. W.; Richter, W. *Langmuir* **1992**, *8*, 2629.
(19) Strey, R.; Schomäcker, R.; Roux, D.; Nallet, F.; Olsson, U. *J. Chem. Soc., Faraday Trans.* **1990**, *86*, 2253.
(20) Strey, R.; Winkler, J.; Magid, L. *J. Phys. Chem.* **1991**, *95*, 7502.
(21) Pedersen, J. S.; Posselt, D.; Mortensen, K. *J. Appl. Crystallogr.* **1990**, *23*, 321.
(22) Tiberg, F.; Malmsten, M.; Linse, P.; Lindman, B. *Langmuir* **1991**, *7*, 2723.
(23) Schmolka, R. Polyalkylene Oxide Block Copolymers. In *Nonionic Surfactants*; Schick, M. J., Ed.; Marcel Dekker Inc.: New York, 1967; Chapter 10, pp 300−371.
(24) Hecht, E.; Hoffmann, H. *Colloids Surf. A* **1995**, *96*, 181.
(25) Mitchard, N. M.; Beezer, A. E.; Mitchell, J. C.; Armstrong, J. K.; Chowdhry, B. Z.; Leharne, S.; Buckton, G. *J. Phys. Chem.* **1992**, *96*, 9507.
(26) Hecht, E. Diplomarbeit, Universität Bayreuth, Bayreuth, 1993.
(27) Pandya, K.; Lad, K.; Bahadur, P. *J. Macromol. Sci., Pure Appl. Chem.* **1993**, *A30*, 1.
(28) Bahadur, P.; Pandya, K.; Almgren, M.; Li, P.; Stilbs, P. *Colloid Polym. Sci.* **1993**, *271*, 657.
(29) Hecht, E.; Mortensen, K.; Gradzielski, M.; Hoffmann, H. *J. Phys. Chem.* **1995**, *99*, 4866.
(30) Malmsten, M.; Lindman, B. *Macromolecules* **1992**, *25*, 5440.
(31) Mortensen, K.; Pedersen, J. S. *Macromolecules* **1993**, *26*, 805.
(32) Mortensen, K.; Talmon, Y., to be published.
(33) Porte, G.; Marignan, J.; Bassereau, P.; May, R. *Europhys. Lett.* **1988**, *7*, 713.
(34) Millner, S. T.; Safran, S. A.; Andelman, D.; Cates, M. E.; Roux, D. *J. Phys. (Fr.)* **1988**, *49*, 1065.
(35) Gompper, G.; Schick, M. *Phys. Rev. E* **1994**, *49*, 1478.
(36) Teubner, M.; Strey, R. *J. Chem. Phys.* **1987**, *87*, 3195.
(37) Porte, G.; Delsanti, M.; Billard, I.; Skouri, M.; Appell, J.; Marignan, J.; Debeauvais, F. *J. Phys. II (Fr.)* **1991**, *1*, 1101.
(38) Brdicka, R. *Grundlagen* der Physikalischen Chemie, VEB Deutscher Verlag der Wissenschaften, Berlin, 1981.
(39) Elworthy, P. H.; Florence, A. T.; Rahman, A. *J. Phys. Chem.* **1972**, *76*, 1763.
(40) Anderson, D.; Wennerström, H. *J. Phys. Chem.* **1990**, *94*, 8683.

MA9504577